# N91-26615

## Chapter 2

# RADAR PRINCIPLES

Toru Sato

Radio Atmospheric Science Center
Kyoto University, Uji, Kyoto 611, Japan

## 1 Introduction

Radar is a general technique, which has a wide range of variability depending on the type of targets to be measured. A radar can be designed to measure a bullet, while another may observe a planet. The radio frequency spectrum employed also spreads out over many decades.

The target of radars described here is the earth's atmosphere. More precisely, it is so called *clear air echoes* from the earth's atmosphere produced by fluctuations of atmospheric index of refraction. We will refer this kind of radar as the *atmospheric radar* here. There is also a category of radar called *weather radar*, which observes precipitation as its principal target. Although much is common, in principle, to the weather radar and the atmospheric radar, we do not discuss the former here. Those who are interested in weather radars are referred to standard text books such as Battan (1973) or Doviak and Zrnić (1984).

It is possible for powerful weather radars to observe the clear-air echoes. Actually, the name clear-air echo is given in the history of development of the weather radar to classify echoes from unknown targets. Above mentioned text books also discuss about the clear-air echoes in some details, but the major difference between their approach and ours is simply that we discuss radars specially designed to observe the clear-air echoes. As we will see later, this difference affects the choice of frequency, requirement on the sensitivity, and the way data are processed. As a consequence, these two types of radars often look surprisingly different.

Weather radar usually use frequencies of SHF band (3–30 GHz), while atmospheric radars make use of much lower HF (3–30 MHz), VHF (30–300 MHz), or UHF (300 MHz–3 GHz) bands. Antenna size of weather radars is a few to about ten meters in diameter, but an atmospheric radar may require a diameter of more than a hundred meters, depending

on its target region. Operational atmospheric radars have antennas with diameter of 10–300 m. Weather radars cover a wide horizontal area of up to several hundred kilometers in radius by scanning their antenna with low elevation angle. Most of atmospheric radars, in contrast, observe narrow angular range around the zenith, but with larger vertical coverage than the weather radars. The hardware of atmospheric radars is examined in detail in a separate chapter.

It should be noted that the atmospheric radars can, at least in principle, and often in reality, also observe precipitation echoes, which is one of important applications of the atmospheric radars.

Atmospheres of other planets can be, in principle, observed by a similar way as those discussed here. However, the extremely large distance between the radar and the target will cause many problems peculiar to such an application. It is also possible to design a radar to observe clear-air echo on board the vehicles such as ships, airplanes, and satellites. Additional Doppler shifts due to motion of the vehicles will be one of major problems, as well as the problem of size limitations, in such cases.

In the following sections, basic characteristics of echoes are examined, and important concepts concerning techniques of the atmospheric radar are introduced.

# 2 The Target

One of important features which make the atmospheric radar unique and different from other kinds of radars is that it observes basically transparent earth's atmosphere. We examine here the nature of the atmosphere as a target of radar.

## 2.1 Vertical Structure of the Atmosphere

The target of the atmospheric radars is the entire earth's atmosphere which extends from the ground (or ocean surface) to the upper boundary of the atmosphere which is usually defined as the highest region rotating together with the earth, whose height ranges from 20,000 km to 40,000 km. Of course, this upper boundary has not yet been observed by means of radar, and only a few of existing radars can observe the atmospheric region above 1,000 km height, most of others with much poorer sensitivity. The lowest observable height, which is usually limited by the switching speed from transmission to reception, ranges from a few hundred meters to several kilometers.

The atmosphere shows a significant variation in its nature even within this limited height range of 0–1,000 km. The largest distinction is between neutral and ionized atmospheres, which are roughly separated by a height of around 100 km. Below this height, the atmosphere is treated as a neutral fluid, while ionized plasma plays an important role above it. These two regions had long been studied independently, and it was widely understood only recently that both can be studied with the same principle.

The other common way of dividing regions is the one based on the vertical structure of atmospheric temperature. Figure 1 shows a typical temperature profile, which is a model profile of mid-latitude equinox taken from the U. S. standard atmosphere (1976). The right ordinate shows the atmospheric pressure in millibars. The atmosphere is classified into 4 regions of troposphere, stratosphere, mesosphere, and thermosphere in ascending order of height.

The troposphere is characterized by a constant decrease in temperature with height. The lapse rate of the model is 6.5 K km$^{-1}$. The main heat source for this region is the solar radiation absorbed by the surface of the earth. Temperature ceases to decrease at 10–15 km, at the tropopause. The height of the tropopause has a clear latitudinal variation, being highest in the equatorial region and decreasing with increasing latitude.

The stratosphere is the region in which temperature increases with height. The stable stratification of the air due to positive temperature gradient accounts for the origin of the name of this region. Temperature reaches its maximum of about 270 K around 50 km at the stratopause height. The heat source for this maximum is the absorption of solar
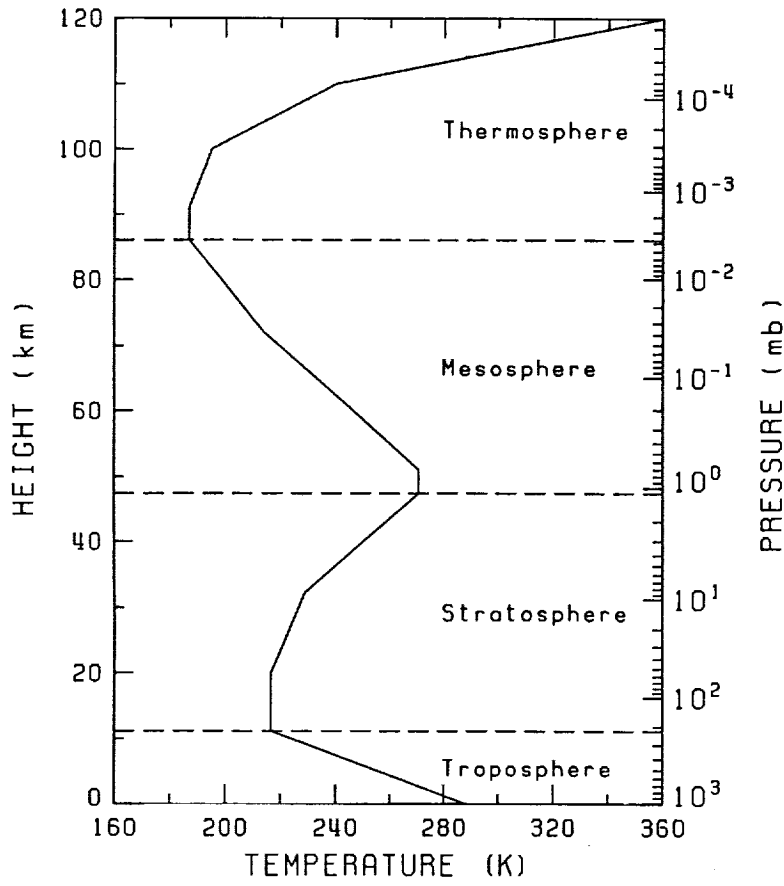
**Fig. 1.** A model temperature profile for mid-latitude equinox (taken from the U. S. standard atmosphere, 1976).

ultraviolet radiation by ozone.

Temperature decreases again in the mesosphere until it reaches the minimum of 180–190 K at the mesopause height of 80–90 km. The heat balance in this region is determined by the radiative heating of molecular oxygen and infrared radiative cooling of carbon dioxide.

Above 80–90 km, the temperature increases monotonically with height to the limit of 1,000–2,000 K due to radiative heating of atomic oxygen *etc.* This region is called the thermosphere in this nomenclature, but it also corresponds to the ionosphere in the above distinction.

## 2.2  Radio Refractive Index

Characteristics of the atmosphere seen by radio waves in the absence of liquid water is expressed in terms of the refractive index $n$. As is the case of optics, $n$ is defined as

$$n = \frac{c}{v}, \tag{1}$$

where $c$ is the speed of light in free space and $v$ is the velocity of the radiowave in the air. Macroscopic changes of $n$ in space cause refraction or reflection, and microscopic changes cause scattering, the latter being of major concern to the atmospheric radar.

Although we are interested in the fluctuations of $n$ from its background, it is important to examine what determines the background $n$. Major contributions to $n$ at frequencies of HF through UHF bands are expressed approximately as (Balsley and Gage, 1980)

$$n - 1 = \frac{3.75 \times 10^{-1}e}{T^2} + \frac{7.76 \times 10^{-5}P}{T} - \frac{N_e}{2N_c}, \tag{2}$$

where $e$ (mb) is the partial pressure of water vapor, $P$ (mb) is the total atmospheric pressure, $T$ (K) is the absolute temperature, $N_e$ is the number density of electrons, and $N_c$ is the critical plasma density.

The first term represents the contribution from water vapor. As is well known, the water molecule has a dipole moment, which varies with frequency. At extremely high frequency of visible light, only the polarized electric field of the water molecules counts for the refractivity. At lower frequencies of radiowave, the water molecules are not only polarized but they also reorient themselves rapidly enough to follow the changes of electric field. As a result, the contribution of the water vapor to $n$ is greater for radio than for optical frequencies (Battan, 1973).

Above the tropopause height of 10–15km, the partial pressure of water vapor becomes negligibly small. The second term due to dry air becomes dominant at this region. Since

the major constituents of the earth's atmosphere, $N_2$ and $O_2$, do not change their mixing ratio largely throughout the middle atmosphere of up to around 100 km, the coefficient stays unchanged. Unlike the first term due to the water vapor, this term is frequency independent, being the same for light and radio waves.

While these two terms concern the neutral atmosphere, the third term gives the contribution from free electrons. This term is negligible below about 50 km, but is dominant at ionospheric heights of above around 80 km. It should be noted here that Eq. 2 gives an approximation valid only when $N_c \gg N_e$, and the effect of the third term is expressed more precisely as

$$n = \sqrt{1 - \frac{N_e}{N_c}},$$

(3)

The critical electron density $N_c$ thus determines the condition with which total (or perfect) reflection occurs in the ionosphere. It is given in MKS units by

$$
\begin{aligned}
N_c &= \frac{4\pi^2 \epsilon_o m_e}{e^2} f^2 \\
&= 1.24 \times 10^{-2} f^2,
\end{aligned}
$$

(4)

where $\epsilon_o$ is the dielectric constant in free space, $m_e$ and $e$ are the mass and the charge of an electron, respectively, and $f$ is the radar frequency ($e.g.$, Stix, 1962). The electron density $N_e$ in the ionosphere usually takes its maximum value of $10^{11}$–$10^{12}$ m$^{-3}$ at 200–400 km height. If $N_c$ is smaller than this maximum, the radiowave is reflected at some height where the condition $N_e = N_c$ is met. Otherwise, the entire energy associated with the radiowave is radiated out of the earth's atmosphere except for a tiny fraction absorbed or scattered by the atmosphere. Under most of ionospheric conditions, $N_c$ is larger than $N_e$ at all heights for frequencies of VHF or higher.

Figure 2 shows a typical variation of these three terms with height. The pressure and temperature are taken from the U.S. standard atmosphere (1976). The saturation pressure is used for the water vapor. The electron density is adopted from Mechtly $et$ $al.$ (1972).

## 2.3  Fluctuations of the Refractive Index

In the absence of total reflection, scattering from fluctuations in the refractive index $n$ dominates the received echo of the atmospheric radar. Statistical fluctuations of the electron density due to random thermal motion of electrons and ions can be strong enough in the ionosphere to cause detectable scattering. This component is called *incoherent scattering* because scattered wave from individual electrons are random in phase, so that
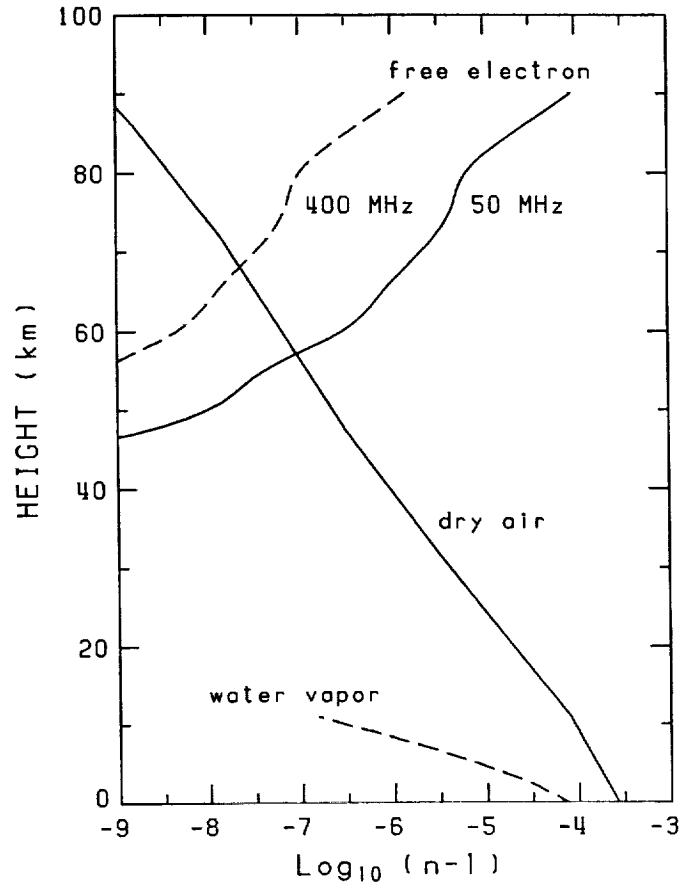
**Fig. 2.** Typical height profiles of water-vapor, dry-air, and free-electron contributions to the radio refractive index $n$.

they add up incoherently. Received echo power is then proportional to the number of electrons illuminated by the radar.

Fluctuations due to atmospheric turbulence is known to be the major source of scattering in the lower and the middle atmosphere. This component is often called *coherent scattering* in contrast to the incoherent scattering in the ionosphere. The main difference of the coherent scattering from the incoherent scattering is that the fluctuation of $n$ is caused by macroscopic motion of air parcels, each of which contains a large number of molecules and/or electrons which contribute to the scattered electric field coherently in phase. As a result, the scattered echo power is roughly proportional to the square of the number density of scatterers instead of the linear proportionality of the incoherent scattering. This substantial enhancement in the echo power is the basis for the MST (Mesosphere Stratosphere Troposphere) radars being able to observe the neutral atmosphere with a relatively small system compared to powerful incoherent-scatter radars.

A large difference of the atmosphere from other targets of radars is its distributed nature. While usual targets as airplanes, ships, cars, or missiles, which are referred to as *hard targets* based on their physical nature, have clear boundary, which enables identification of the target, it is usually absent in spatial distribution of the echo from the atmosphere. It is thus necessary to distinguish parts of the atmosphere by means of spatial coordinates of direction and range. This type of target is often called as the *soft target*.

A direct consequence of this limitation, for example, is the fact that decreasing the size of identified volume in order to improve spatial resolution results in a decrease in the echo power, and thus a decrease in sensitivity. On the other hand, the rate of decrease of the echo power with increasing range to the target is much slower with the soft target than with the hard target, because the volume, and thus the size of the scatterer, usually increases with increasing range in case of the soft target.

Mathematical relations which determine the strength of the echo are derived in the following section.

# 3 The Radar Equation

In designing a radar system, we first need to know how strong the echo of interest is. We will derive a relation between transmitted and received power, called the radar equation, for various situations which concern observations with the atmospheric radar.

## 3.1 The Radar Equation for a Hard Target

Before discussing the scattering from fluctuations in the radio refractive index, let us first examine a simpler case of the scattering from an isolated hard target located in free space. Suppose we transmit radiowave of power $P_t$ out of an omni-directional antenna which radiates the power into all directions with uniform strength. The density of the power $P_i$ passing through a unit area located at a point sufficiently far from the antenna and perpendicular to the direction of propagation is given by

$$P_i = \frac{P_t}{4\pi r^2}, \tag{5}$$

where $r$ is the distance of the point from the transmitting antenna. The antenna used for a radar usually has a strong directivity with which a narrow region can be illuminated selectively. The above equation is thus modified as

$$P_i = \frac{P_t G_t}{4\pi r^2}, \tag{6}$$

where $G_t$ is the *directional gain*, or simply, the gain, of the antenna, which is a function of the azimuth and the zenith angles.

We now consider a target located at this point which intercepts the power and scatters it into various directions. The density of the scattered power $P_s$ per unit area at a distance $r'$ from the target is expressed in terms of the *scattering cross section* $\sigma$ of the target as

$$P_s = \frac{P_i}{4\pi r'^2}\sigma, \tag{7}$$

where $\sigma$ is defined as an effective area of the scatterer, the power illuminating which area is scattered isotropically. It should be noted that an alternate parameter of the *differential scattering cross section* $\sigma_d \equiv \sigma/4\pi$ which expresses the scattered power per unit area and *per unit solid angle* is also used often, and occasionally the difference is not clearly mentioned.

It is known, for example, that a perfectly conducting sphere with a radius much larger than the wave length of the radar has a scattering cross section equal to its physical cross section (*e.g.*, Skolnik, 1980).

If we receive the scattered power with an antenna which has a capability of collecting all power passing through an *effective area* $A_e$, the received power $P_r$ is expressed as

$$P_r = P_s A_e L, \tag{8}$$

where $L$ is the loss factor which represents various attenuation of the received signal due to antenna, transmission line, connectors *etc*. By combining Eqs. 6–8, we obtain

$$P_r = \frac{P_t G_t A_e L}{(4\pi r^2)(4\pi r'^2)} \sigma. \tag{9}$$

This equation gives the received echo power from a given target by a radar, and hence is called the *radar equation*. We have so far considered a general case in which the transmitting and the receiving antennas are not the same. Although this type of radar, which is called the *bistatic radar*, or the *multi-static radar* in case there are more than one receiving antennas, is used in reality for some applications, it is much more common to use the same antenna both for transmission and reception for simplicity. This type of radar which uses a single antenna is called the *monostatic radar*, and we will limit our discussion below to this type of radars.

The two parameters $G_t$ and $A_e$ used in the above equations seem to indicate, at a first look, distinct properties of an antenna. There is, however, a useful universal relation known between the two (Silver, 1951), which is

$$G_t = \frac{4\pi A_e}{\lambda^2}, \tag{10}$$

where $\lambda = c/f$ is the radar wavelength. Although $A_e$ is a function of direction since $G_t$ is so, it is implicitly assumed that the antenna beam of the radar is pointed to the direction of the target, so that both $G_t$ and $A_e$ take their maximum value.

For a monostatic radar, the radar equation thereby reduces to

$$P_r = \frac{P_t A_e^2 L}{4\pi \lambda^2 r^4} \sigma. \tag{11}$$

This equation gives the basis for radar system design of choosing appropriate transmitter power $P_t$ and effective antenna area $A_e$ for a given target with a scattering cross section $\sigma$ at a range $r$.

The minimum detectable power $P_r$ is limited by the noise power $P_n$ which contaminates the received signal from the target. In most cases, the dominant component of the noise is the *white noise* which is defined as a random time series of signal with a uniform frequency power spectrum within the receiver bandwidth $B$. The power of white noise produced by a resistor at a temperature $T$ and for a given bandwidth $B$ is given by (Dicke *et al.*, 1946)
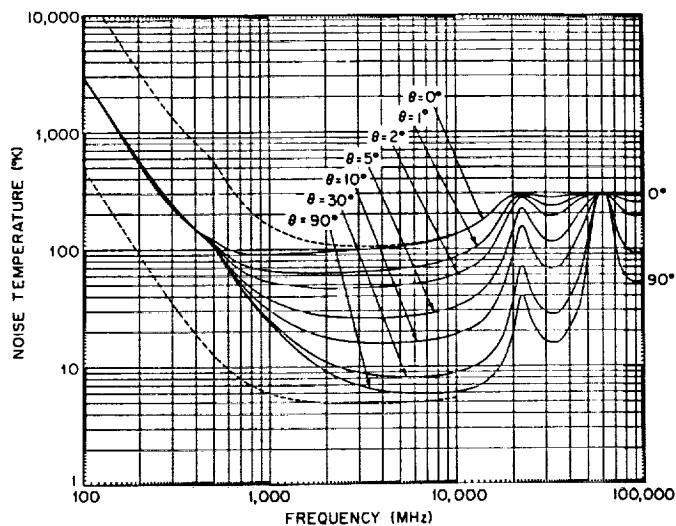
$$P_n = kTB \tag{12}$$

Fig. 3. The sky noise temperature versus frequency (after Skolnik, 1970).

where $k$ is the Boltzmann constant ($= 1.38 \times 10^{-23}$ WsK$^{-1}$).

Since this formula can be applied to any type of white noise, it is common to express the noise power of the radar in terms of this equation where $T$ is called the *equivalent noise temperature*. This noise temperature represents all kind of noise sources, and is decomposed as

$$T = T_s L + T_r \tag{13}$$

where $T_s$ is the sky noise temperature due to cosmic, solar, and atmospheric radiation, $L$ is the loss factor, and $T_r$ is the noise power generated by the receiver itself. The sky noise temperature varies largely depending on the radar frequency and also on the direction of the antenna beam. Figure 3 illustrates it versus frequency (after Skolnik, 1970). Solid curves are for various elevation angle $\theta$ of the antenna beam direction for geometric-mean galactic temperature, sun noise ten times quiet level, sun in unity-gain side lobe, cool temperate-zone troposphere, and 2.7 K cosmic black body radiation. The upper dashed curve is for maximum galactic noise at the center of galaxy, sun noise 100 times quiet level, zero elevation angle, and other factors the same as for the solid curves. The lower dashed curve is for minimum galactic noise, zero sun noise, and elevation angle of 90°. The maxima at 22 and 60 GHz are due to water-vapor and oxygen absorption resonances.

## 3.2   The Radar Equation for Distributed Targets

The radar equation derived above applies to a single target. If there are more than one target in the same volume $V$ of the air observed by a radar, the received electric field is expressed as the sum of the electric field components caused by individual scatterers. For a situation where they are random and have no correlation between each other, the total received echo power becomes the sum of the echo power from individual scatterers. In this case, the scattering cross section $\sigma$ in Eqs. 7, 9, and 11 are simply replaced by $\Sigma\sigma$. If the number of scatterers is very large and if scatterers are distributed uniformly in space, $\sigma$ increases linearly as $V$ increases. It is thereby suitable to define the *volume reflectivity* $\eta$, or the scattering cross section per unit volume as

$$\eta \equiv \frac{d\sigma}{dV}. \tag{14}$$

It should be noted that $\eta$ has a dimension of $[\mathrm{m}^{-1}]$ unlike the ordinary reflectivity, which is dimensionless.

This situation applies, for example, to the incoherent scattering due to free electrons in the ionosphere observed with a sufficiently high frequency of above about 1 GHz, for which the volume reflectivity is given by

$$\eta = N_e \sigma_e, \tag{15}$$

where $\sigma_e$ is the scattering cross section of an electron, which is given by

$$\begin{aligned} \sigma_e &= \frac{e^4}{4\pi\epsilon_0^2 m_e^2 c^4} \\ &= 9.98 \times 10^{-29} \quad (\mathrm{m}^2). \end{aligned} \tag{16}$$

The condition 'sufficiently high frequency' is necessary because otherwise interactions between electrons and ions through the Coulomb forces modify significantly the motion of the electrons reacting to the radar wave field. For a sufficiently low frequency of VHF and lower UHF bands, an extra coefficient of 1/2 should be multiplied to the right-hand side of Eq. 15 (Fejer, 1961).

This type of approach based on a microscopic viewpoint is practical only for idealized situations as discussed above. We need to treat the problem from a more macroscopic viewpoint of regarding scattering as due to fluctuations in the refractive index $n$ in order to discuss the cross section of the neutral atmosphere. Here $n$ is a continuous function of space, and represents all of the effects caused by scatterers.

The scattered power $P_s$ produced by small fluctuations of the refractive index $\Delta n$ is expressed formally as (e.g., Doviak and Zrnić, 1984)

$$P_s = \frac{k^4 P_i}{4\pi^2 r^2} \left| \int_V \Delta n \exp(i2\mathbf{k} \cdot \mathbf{r}) dV \right|^2, \tag{17}$$

where $k$ $(= 2\pi/\lambda)$ is the radar wavenumber, $\mathbf{k}$ is the propagation vector, and $\mathbf{r}$ is the radius vector to a point in the scattering volume. By comparing Eq. 17 with Eq. 7, and applying Eq. 14, we obtain

$$\eta = \frac{k^4}{\pi}C \tag{18}$$

$$C = \frac{1}{V}\langle\left|\int_V \Delta n \exp(i2\mathbf{k}\cdot\mathbf{r})dV\right|^2\rangle$$

where $\langle\rangle$ denotes an ensemble average. Although this equation gives a universal expression for the scattering cross section and the volume reflectivity, it is not easy, in general, to perform the integration to determine $C$. Specific results will be presented in a separate chapter.

For a uniformly distributed target, $V$ is determined by the spatial resolution of the radar. Namely, for a radar with a circular antenna, it is expressed in terms of the half-power beam width of the antenna $\theta_h$ in radians, and the size of the range cell $\Delta r$, which is examined in the next section, as

$$V = \pi(\frac{r\theta_h}{2})^2\Delta r. \tag{19}$$

The beam width of the antenna has a direct relation with the gain of the antenna $G_t$ because both of these parameters express the degree of concentration of the transmitted power of the radar in space. Probert-Jones (1962) expressed the relation as

$$G_t = (\frac{\pi a}{\theta_h})^2, \tag{20}$$

where $a$ is a non-dimensional factor which concerns the non-uniformity of illumination of the antenna. Combining this equation with Eq. 10 we obtain

$$\theta_h = \frac{a\lambda}{D_e} \quad \text{(rad)}, \tag{21}$$

where $D_e$ is the effective diameter of the antenna given by $\sqrt{4A_e/\pi}$. For a circular array antenna with uniform excitation for which $D_e$ is roughly equal to the physical diameter of the antenna, $a = 1$ gives a good approximation.

With the aid of Eqs. 10, 19, and 20, the radar equation Eq. 11 can be rewritten for distributed targets as

$$P_r = \frac{P_t A_e \pi a^2 \Delta r L}{64r^2}\eta. \tag{22}$$

Comparison of this equation with Eq. 11 for a hard target immediately reveals a few of interesting features of the scattering from distributed targets. First of all, the proportionality of the received echo power on the range $r$ is to the square, not to the

forth power as is the case for a hard target. This means that the echo power decreases relatively slowly with increasing $r$, as mentioned in the preceding section.

Secondly, $P_r$ depends only linearly on the effective antenna aperture $A_e$. While the $A_e^2$ factor in Eq. 11 counts for the antenna gain both for transmission and reception, the linear dependence in Eq. 22 can be interpreted that all of the radiated power is intercepted by the distributed scatterers, and thus the antenna gain does not count during transmission. It should also be noted that Eq. 22 does not contain any factor which contains a dependency on the radar frequency. These properties makes the *power aperture product* $P_t A_e$ a good indication of the sensitivity of an atmospheric radar.

Finally, the $\Delta r$ term in Eq. 22, which does not appear in Eq. 11 means that any attempt to improve the range resolution of an atmospheric radar should be made at an expense of reduced sensitivity.

## 3.3 The Radar Equation for Specular Echoes

We have so far considered two extreme cases of a single target and uniformly distributed target. Although it is not the purpose of this chapter to get into details of various scattering mechanisms, let us examine a few more cases for which the radar equation takes alternate forms.

The first example is the *Fresnel (or partial) reflection* induced by a horizontal layer which has a slightly different refractive index from that of surrounding air and extends over a sufficiently wide area. This layer can be treated like a planar mirror, but with a small reflectivity $\rho$ for incident electric field (Friend, 1949). Note that $\rho$ here is the reflectivity in an ordinary sense which has no dimension, and has a complex value of $|\rho| \leq 1$.

The derivation of the radar equation for this case is rather simple, because we can consider the case to be a one-way transmission from an antenna to its mirror image located at a distance $2r$, with an extra power loss factor of $|\rho|^2$. Figure 4 shows the situation schematically. The received power is thus given by

$$
\begin{aligned}
P_r &= \frac{P_t G_t}{4\pi(2r)^2} A_e L |\rho|^2 \\
&= \frac{P_t A_e^2 L}{4\lambda^2 r^2} |\rho|^2
\end{aligned}
\tag{23}
$$

Although the echo power depends on the range by $r^2$ like the case of distributed targets, it is proportional to $A_e^2/\lambda^2$ like that of a hard target. One of important aspects of the Fresnel reflection is its aspect sensitivity. The above equation assumes that the antenna beam is directed perpendicular to the layer, for which the received echo takes its maximum value.
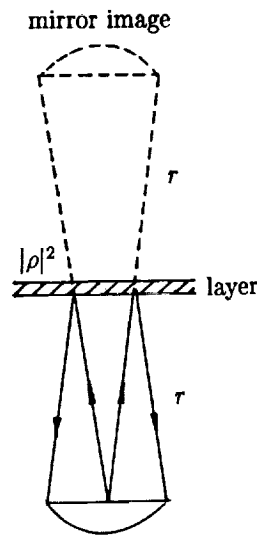
**Fig. 4.** Equivalent ray path for the Fresnel reflection. The dashed lines denotes the mirror image of the radar due to the layer.

The echo power falls off rapidly as the angle of the antenna beam is changed from this position. The rate of decrease is a function of the beam width of the antenna, and can be readily computed by considering the relation between the transmitting antenna and its mirror image due to the layer. It is not so easy, however, to calculate this function when the layer has some roughness of the order comparable to or larger than the wavelength. Such situation needs a more rigorous treatment based on Eq. 17.

We next examine a case where the scatterer has a linear shape in space. The most important application of such case is the reflection from *meteor trails* which appear at around 100 km height. Meteor trail is a strong localized ionization produced along a path of a meteor caused by the frictional heating when it penetrates into the earth's atmosphere. Since the echo is strong enough to be detected with relatively low sensitivity radars, it has been extensively studied (*e.g.*, McKinley, 1961). There is a category of atmospheric radar called the *meteor radar* which makes use of the meteor echoes to investigate the dynamics of the lower part of the ionosphere.

The scattering element in this case is an electron as is the case for the incoherent scattering for which element the radar equation is given in the form of Eq. 11 by

$$P_{r0} = \frac{P_t A_e^2 L}{4\pi \lambda^2 r^4} \sigma_e. \tag{24}$$
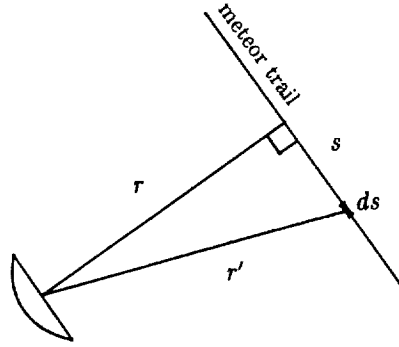
**Fig. 5.** Coordinates for deriving the effective length $l_e$ for scattering from a meteor trail.

Unlike the case of incoherent scattering where contributions from individual electrons add up randomly, scattered electric fields from electrons aligned in space have a strong coherence. Since the effective diameter of the meteor trail which affects the scattering is shorter than the wavelength of meteor radars, we can safely assume that all electrons are aligned on one line with a *line density* of $q_e$ (m$^{-1}$). We also assume a straight line without any curvature for simplicity, and that the line is located sufficiently far from the radar.

Electric-field contributions from electrons at distinct points on the line have similar amplitude, but have various phase. We introduce an idea of the *effective length* defined by

$$l_e \equiv \left| \int_{-\infty}^{\infty} \exp\{-i2k(r' - r)\} ds \right|, \tag{25}$$

where $r$ is the distance of the line from the radar, and $r'$ is the range of a line element $ds$ on the line. Figure 5 shows the coordinates. The idea is to represent contributions from all parts of the line which have distinct phases by an effective length in which contributions are assumed to have the same phase at the receiving antenna. By making an approximation $r' - r \simeq s^2/(2r)$ where distance $s$ is measured along the meteor trail from the perpendicular point, we obtain

$$l_e = \sqrt{\frac{r\lambda}{2}}. \tag{26}$$

Since the number of electrons within $l_e$ is $l_e q_e$, and since the electric fields of scattered waves from these electrons have the same phase, the total echo power is given by

$$
\begin{aligned}
P_r &= (l_e q_e)^2 P_{r0} \\
&= \frac{P_t A_e^2 L}{8\pi\lambda r^3} \sigma_e q_e^2. \tag{27}
\end{aligned}
$$

This equation has a range dependence of $r^{-3}$ which lies between the cases of a hard target and distributed targets.

## 3.4  Near Field Correction

In deriving these radar equations, we have assumed that the target is located at a point 'sufficiently far' from the radar without giving any explicit reason or quantitative limit for it. Here we examine how large should be the range $r$ in order that equations we have derived are valid, and what happens within this limit.

The antenna of an atmospheric radar is, whether it is an dish antenna as a paraboloid or an array of Yagi's or half-wave dipoles, designed to form a beam of the transmitted wave as sharp as possible, because it is the condition to maximize the gain $G_t$ and effective area $A_e$ as shown in Eqs. 20 and 21. In order to make the beam sharp, it is essential to produce a planar wavefront over the antenna aperture to the extent as wide as possible. The transmitted wave thereby propagates as a plane wave at a distance near the antenna without changing its outer boundary which keeps the shape of the antenna aperture. As it propagates further, it gradually spreads out into a conical region and finally forms a spherical wave with its center located at the center of the antenna aperture.

The region where the wave can be regarded as a planar wave is called the *near field* of the antenna, while the region where it is a spherical wave is called the *far field*. In another word, the far field is a region from which the antenna can be seen as a point. This condition is stated mathematically that the distance of a target point measured from any point on the antenna aperture falls within a difference sufficiently smaller than the wavelength.

Conventionally, the boundary between the near field and the far field is defined as a range where the cylinder with a diameter equal to the diameter $D$ of the antenna intercepts the cone with an angle $\theta_h$ and with its apex located at the center of the antenna as shown in Figure 6. This range $r_o$ is given by

$$r_o = \frac{D^2}{\lambda},\qquad(28)$$

at which the difference of the distance measured from the center and from an outer edge of the antenna aperture becomes $\lambda/8$. As is shown in Eq. 28, $r_o$ is a function of the diameter of the antenna and the radar frequency. The largest value of $r_o$ associated with the existing atmospheric radars is 129 km for the Arecibo UHF radar, which operates at 430 MHz and has an antenna with a diameter of 300 m. All regions of the atmosphere except the upper ionosphere falls within the near field for such case. On the other hand, $r_o$ is much smaller for VHF radars. The MU radar of Japan, for example, operates at
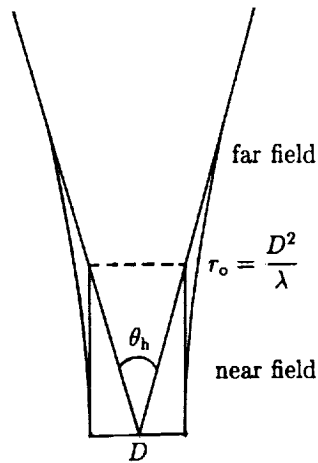
**Fig. 6.** A conventional definition of the boundary between the near field and the far field.

46.5 MHz and has a 103 m antenna, for which $r_o$ is only 1.6 km. Since the minimum height (or range) that the MU radar can observe is about 1.5 km, the far field condition almost always holds.

In the near field of an antenna, Eq. 6 should be thereby rewritten as

$$P_i = \frac{P_t}{A_e}. \tag{29}$$

Also, Eq. 8 should be modified because the phase differences of the received waves on different parts of the antenna aperture, which differences cause interference and thus reduction of the echo power, is important for the case of the near field. The effective area $A_e$ should then be replaced by an area which represents the effect of adding waves with different phases. This area is obtained by a consideration similar to that of Eq. 26 for the effective length of the reflection from a meteor trail, and is given by $\pi \lambda r / 4$. This area also agrees with that of the *first Fresnel zone* which is defined as a zone on a plane in which a wave radiated from a point source arrives with a phase difference of less than $\pi/2$. Figure 7 shows the situation schematically. Thus Eq. 8 becomes

$$P_r = \frac{P_s \pi \lambda r L}{4}. \tag{30}$$

With Eqs. 29 and 30, the radar equation for a hard target Eq. 11 is rewritten as

$$P_r = \frac{P_t \lambda L}{16 A_e r} \sigma. \tag{31}$$

The most striking feature of this equation is that the received power is inversely proportional to the effective area of the antenna, meaning that a smaller antenna gives a stronger
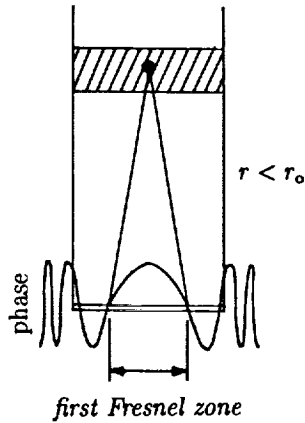
*first Fresnel zone*

**Fig. 7.** Scattering due to a hard target within the antenna near field.

echo than a larger one. This is due to the fact that the power density of the transmitted wave is higher for smaller antenna as far as the target is within the near field. It should be noted, of course, that the upper boundary $r_o$ of the near field also decreases as the size of the antenna is reduced. The other important difference is that the echo power decreases only by $r^{-1}$ with increasing range $r$ in contrast to the very steep $r^{-4}$ decay shown by Eq. 11.

Similarly, the radar equation for distributed targets Eq. 22 can be modified for the case of the near field. Besides the corrections we have made, the scattering volume expressed by Eq. 19 should also be changed as

$$V = A_e \Delta r. \tag{32}$$

Applying Eqs. 14 and 32 to Eq. 31, we obtain the radar equation for distributed targets within the antenna near field:

$$P_r = \frac{P_t \Delta r \lambda L}{16r} \eta. \tag{33}$$

Note that this equation contains no dependence on the antenna size parameter. What Eqs. 31 and 33 tells us is that increasing the size of the antenna in order to improve the sensitivity of the radar works only for targets outside the near field of the antenna.

In section 3.3, we also made an implicit assumption that the effective size of the target for specular reflections, which is determined by phase coherence of the scattered electric field, is smaller than the lateral dimension of the beam at that range. It can be shown that the range at which $l_e$ for the meteor trail becomes the same as the beam size is coincidentally given by $r_o$. The $\sqrt{r}$ dependence of $l_e$ thereby verifies the use of Eq. 27 for

$r > r_o$. A similar condition $r > r_o/2$ can be derived for the validity of Eq. 23 for Fresnel reflection by considering the condition that the size of the first Fresnel zone of the mirror image becomes larger than the size of the antenna.

# 4 Basic Techniques

The radar equation derived in the previous section tells us the intensity of echo, which is essential to estimate the necessary transmitter power and the antenna aperture, but nothing more. In this section, we briefly survey basic techniques used in the atmospheric radar in determining the range of desired target and also in deriving other information concerning the target. Details of individual technique will be discussed in following chapters.

## 4.1 Pulsed Waveforms

*Ranging*, or measurement of the range to a target, is one of important functions of radar. We, again, start with the case of observing a hard target. The ranging is made by measuring the time delay of the received echo from the target with respect to the transmitted signal.

As far as the refractive index $n$ satisfies $|n-1| \ll 1$, speed of the radio wave can be well approximated by that in free space as shown by Eq. 1, the error of which approximation is given by Eq. 2. In the lower and the middle atmosphere of below about 100 km, $|n-1| < 10^{-3}$ as shown in Fig. 2, thence the error is negligible for all practical applications. The error becomes larger, however, in the ionosphere of above 100 km depending on the frequency $f$ and the electron density $N_e$ as shown by Eqs. 3 and 4. At a relatively low frequency of 50 MHz, for example, the maximum value of $n - 1$ during daytime reaches $\sim -0.02$ at around the peak height of F2 region of 200–300 km. A care must be taken of this error for an accurate ranging of a hard target above the ionospheric height using lower VHF band. For oblique beam waves, refraction of the ray path is not negligible either under such condition.

Assuming $n = 1$, the range $r$ of a stationary point target is given by

$$r = \frac{c\tau}{2},\tag{34}$$

where $\tau$ is the time delay of an echo. In order to measure this time delay, we need to add some 'feature' to the transmitted wave so that a part of the wave can be identified from others. Although there are a variety of ways to do this, many of which are of practical use, the simplest and most widely used way is to transmit a short pulse of a waveform

$$E(t) = \begin{cases} E_o \sin(2\pi f t) & (0 \le t \le \Delta t) \\ 0 & (t < 0, \ t > \Delta t) \end{cases},\tag{35}$$

where $E_o$ is the amplitude of the electric field of the wave. It should be noted that it is not common to use such an idealized waveform in a real radar because of various restrictions,

so that the amplitude $E_o$ is usually a smoother function of time than this one. When we transmit a pulse of length $\Delta t$ sec, we receive the echo from this pulse for a duration of $\Delta t$ sec right after a $\tau$ sec of delay. Since we measure the delay in terms of the range according to Eq. 34, this duration is interpreted as if the target has a finite length

$$\Delta r = \frac{c\Delta t}{2} \qquad (36)$$

in the radial direction, which length is called the *range resolution*.

It is thereby necessary to reduce $\Delta t$ in order to improve the range resolution. Unfortunately, however, there is a conflicting relation between the length of the pulse and its frequency bandwidth. For a rectangular pulse waveform of Eq. 35, the half-power frequency bandwidth $B$ is given by

$$B = \frac{0.886}{\Delta t}. \qquad (37)$$

Since the receiver should cover this bandwidth, the noise power contaminating the echo increases linearly as increasing $B$ as shown by Eq. 12, thus resulting in a linear decrease of the signal-to-noise ratio, which is, as a consequence, proportional to $\Delta t$.

This dilemma can be solved by means of *pulse compression* which allows a radar to utilize a long pulse without sacrificing the range resolution. The basic idea of the pulse compression is to put extra features within the long pulse so that each part of the pulse can be identified, which idea is just the same as the one used above in introducing the pulsed waveform. This is realized, in this case, by applying further modulation to the already pulse-modulated waveform. Among various ways of modulation, binary phase modulation (or coding) is most widely used for the atmospheric radar application. This form of pulse compression is performed by sending $N$ consecutive pulses with the phase of carrier wave 0 or $\pi$ different from that of the first pulse. The advantage of utilizing only 0 and $\pi$ of the phase is that they can be interpreted as plus and minus signs of the envelope $E_o$, so that no special hardware for phase modulation and demodulation is required. Each component pulse of length $\Delta t$ is referred to as a *sub-pulse* of an $N$-element coded pulse of length $N\Delta t$. The choice of the time series of phases (0 or $\pi$) is a subject of mathematical considerations, and will be discussed in details in a separate chapter (see, for example, Nathanson, 1969, or Skolnik, 1980 for reference).

Here we choose a random phase coding as an example, with which sub-pulses have random and independent phases with each other. The received signal time series from a stationary point target is a weakened and delayed copy of the transmitted time series, which is a series of pulses with a random sequence of signs. We can 'compress' the received signal by displacing sub-pulses to the position of the first sub-pulse with corrected phase,
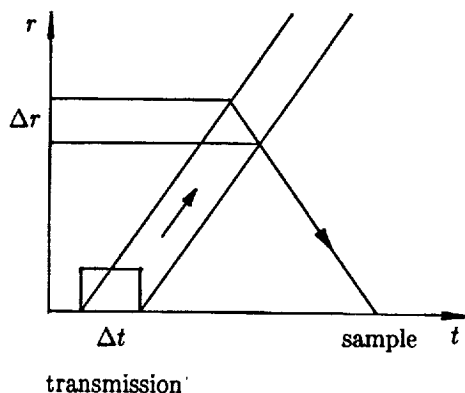
**Fig. 8.** Time-height section showing the relation of the size of a range cell and the length of a pulse for distributed targets.

and by adding them together. Mathematically, this procedure is expressed as taking the cross-correlation of the transmitted and received time series. This procedure enhances the signal power, which has equal phase for all sub-pulses, by $N^2$ times, while the statistically independent noise power only by $N$ times, thence the signal-to-noise ratio by $N$ times.

Since the phases of sub-pulses are random, the entire pulse has the same bandwidth as that of each sub-pulse. The range resolution also stays unchanged because the cross-correlation disappears outside an interval of $\Delta t$ due to random phases between adjacent sub-pulses. As a summary, $N$-element binary phase compression improves the signal-to-noise ratio by $N$ times compared to a single pulse of length $1/N$, without changing the range resolution.

We now consider the case of distributed targets. If the distribution is uniform with range, the received echo power decreases with the time $t$ after transmission of a pulse as $t^{-2}$, which simply reflects the $r^{-2}$ dependence of the radar equation through Eq. 34. The object then becomes to determine the nature of the target at a given range, instead of determining the range of the target. The meaning of the range resolution also should be changed from *the ambiguity in determination of the range of a target* to *the radial size of scattering volume which contributes to the echo at a given time.* Actually, the range resolution $\Delta r$ given by Eq. 36 corresponds to the difference of the range of echoes returned from the leading and trailing edges of a pulse of length $\Delta t$ at the same time of receiving as shown in the time-height section of Figure 8. It is thereby appropriate to call $\Delta r$ as the size of a range cell as already quoted in Eq. 19. Echoes from distinct ranges can be obtained by sampling the received signal at an interval of $\sim \Delta t$. A sampling

interval of less than $\Delta t$ produces overlapping regions between the samples, while a spars sampling results in missing regions. It is therefore common to sample at an interval just equal to $\Delta t$. The sampled time series provides a range (or usually, height) profile of the atmosphere. We should note that the impulsive sampling intended by Fig. 8 does not represent a realistic situation where the receiver has a bandwidth equal to that of the transmitted pulse. In this case, an instantaneous sample of receiver output contains the echo spreads over a duration of $\Delta t$. Although this effect broadens the range cell from a rectangular shape of width $\Delta r$ into a triangular one of width $2\Delta r$, the 'half-power' size of the cell is still given by $\Delta r$.

As we have seen, the signal-to-noise ratio is proportional to the length of pulse $\Delta t$ for the case of a hard target. For the case of distributed targets, we need to take into the account the linear proportionality of echo power on $\Delta r$ as shown in Eq. 22, which represents the number of scatterers in a range cell. The signal-to-noise ratio thus becomes proportional to $\Delta t^2$, setting a severe restriction in improving the range resolution. For example, dividing a single pulse into $N$ sub-pulses with binary phase coding improves the range resolution by $N$ times without sacrificing the signal-to-noise ratio of a hard target, while the same alteration offers the same improvement only at an expense of a reduction of the signal-to-noise ratio to $1/N$ for the case of distributed targets.

## 4.2   The Doppler Principle

We have so far concentrated our attention only to the echo power. Physical meaning of the echo power is, however, clear only for the case of incoherent scattering from the ionosphere, for which case it can be interpreted in terms of the electron density. It is difficult to make use of the echo power from the lower and the middle atmosphere in a quantitative manner in terms of physical parameters of geophysical interests.

The *Doppler shift* of the echoes, on the other hand, has a great importance for these regions as well as for the ionosphere, because it is directly related to the motion of the target, which is wind. The Doppler frequency shift of echoes from a moving target relative to the radar is given by

$$f_{\rm d} = \frac{2f}{c} v_{\rm d}, \tag{38}$$

where $v_{\rm d}$ is the line-of-sight component of velocity vector $\mathbf{v}$ of the target relative to the radar.

Since the maximum velocity encountered in the atmosphere is on the order of $100\ {\rm m\,s^{-1}}$, $|f_{\rm d}| < 1$ kHz for any frequency $f$ of less than 1 GHz. A typical value of $f_{\rm d}$ for 50 MHz band is, for example, around 3 Hz, which corresponds to a line-of-sight velocity of $10\ {\rm m\,s^{-1}}$.

Bandwidth of transmitted pulses is, on the other hand, 100 kHz–1 MHz corresponding to the minimum length of sub-pulses of 1–10 $\mu s$. It is thereby very difficult, if not impossible, to detect such small Doppler shift of a pulse relative to its bandwidth from each received pulse.

Instead, the method of time-series analysis is applied to the series of received signal from consecutive pulses at the same range. If a stationary target is observed, all received pulses should have the same phase relative to the transmitted pulse. It is then interpreted that the received time series has the DC component only, which means that the Doppler shift is zero. Next we suppose that the target is moving at a sufficiently slow speed of $v_d$ in the radial direction so that it does not move out of a range cell into the next one within the period of interest. We examine samples of echoes obtained at the same range cell from adjacent pulses separated by an inter-pulse-period (IPP) of $T$. Then the phase difference $\Delta\phi$ between the two samples is given by

$$\Delta\phi = 2\pi f_d T = \frac{4\pi f T}{c} v_d. \tag{39}$$

This equation can be applied not only to a hard target but also to distributed targets as far as they move with a mean speed of $v_d$. The phase difference can be determined from a pair of pulses, while the Doppler frequency shift $f_d$ can be directly derived by a spectral analysis of the time series of samples taken from many pulses.

A limitation of this method arises from the requirement $|\Delta\phi| < \pi$ so that $f_d$ can be determined without ambiguity, together with the one $T > 2r_{max}/c$ which comes from the restriction that we cannot transmit a new pulse before receiving the echo of the previous pulse from the longest range $r$max of interest. By combining these two requirements, we obtain

$$|v_d| r_{max} < \frac{c^2}{8f}, \tag{40}$$

which gives the condition that both the range and the velocity of a target can be determined unambiguously. Since the quantities on the left-hand side of this equation are limited roughly by 100 m s$^{-1}$ × 100 km = $10^7$ m$^2$s$^{-1}$, this condition is usually satisfied for a frequency of below about 1 GHz, which is the frequency used for atmospheric radars.

Considerations made above assumes that the echo is perfectly correlated in time, which assumption is not valid for the case of the atmospheric radar, where echoes have finite correlation time $\tau_c$ due principally to random motion of scatterers within a scattering volume. This correlation time is inversely proportional to the spectral broadening due to the random motion and other observational effects, and given by

$$\tau_c = \frac{b}{\sigma_f} = \frac{bc}{2f\sigma_v}, \tag{41}$$

where $\sigma_f$ and $\sigma_v$ denote the standard deviation of the random motion in terms of Doppler frequency and radial velocity, respectively, and $b$ is a numerical coefficient of order unity which is determined by the velocity distribution of the random motion. For a Gaussian distribution, $b = 1.18$.

The value of $\sigma_v$ differs largely depending on the height, since it is the order of mean thermal motion of ions of more than $1~\mathrm{km\,s^{-1}}$ in the ionosphere, while it is the mean velocity of turbulent eddies of the order of $1~\mathrm{m\,s^{-1}}$ in the lower and the middle atmosphere. For ionospheric observation, for which $\sigma_v \gg v_d$, the $v_d$ term in Eq. 40 should be replaced by $\sigma_v$, which determines spectral width and thus the minimum sampling interval. It is easily understood that the condition for unambiguous sampling is then no more satisfied, meaning that spectral information of the scatterers must be derived within an interval of order of $\tau_c$. A special technique called *multi-pulse method* was developed for ionospheric observations, and has been widely used (*e.g.*, Farley, 1969).

## 4.3   Velocity Field Measurements

As shown in Eq. 38, velocity of targets measured by a radar with the Doppler technique is a line-of-sight velocity, which is the projection of velocity vector to the radial direction. We will briefly examine here two distinct techniques of determining the three components of the velocity vector: the *Doppler-Beam-Swing* (DBS) method and the *Spaced-Antenna-Drifts* (SAD) method.

The DBS method makes use of multiple antenna beams each of which is oriented to observes the radial velocity at a different direction. The velocity vector is computed from the line-of-sight velocities from these directions. Here we need to make an assumption that the velocity field is uniform in space over the volume which contains the range cells used to compute a velocity vector. In the atmospheric radar application, it is common to determine a velocity vector from line-of-sight velocities of range cells with the same height assuming the uniformity only in the horizontal plane, so that a height profile of the velocity vector can be obtained. This is because the horizontal velocity is usually much larger than the vertical velocity in the stratified earth's atmosphere, thus making the horizontal uniformity of the velocity field much better than in the vertical direction. Also, the fact that the zenith angle of antenna beams is usually kept within about 30°supports this assumption, in contrast to the case of weather radars, which use almost horizontal beam directions,

The line-of-sight component of the wind velocity vector $\mathbf{v} = (v_x, v_y, v_z)$ at a given

height is expressed as

$$v_{\mathrm{d}} = \mathbf{v} \cdot \mathbf{i}$$
$$= v_x \cos \theta_x + v_y \cos \theta_y + v_z \cos \theta_z, \tag{42}$$

where $\mathbf{i}$ is a unit vector along the antenna beam direction, and $\theta_x$, $\theta_y$, and $\theta_z$ are the angle between $\mathbf{i}$ and the $x$, $y$, and $z$ axis, respectively. If we measure $v_{\mathrm{d}}$ at three beam directions $\mathbf{i}_1$, $\mathbf{i}_2$, and $\mathbf{i}_3$ which do not constitute a plane, we can obtain an estimate of $\mathbf{v}$ as

$$\mathbf{v} = \begin{pmatrix} \cos \theta_{x1}, & \cos \theta_{y1}, & \cos \theta_{z1} \\ \cos \theta_{x2}, & \cos \theta_{y2}, & \cos \theta_{z2} \\ \cos \theta_{x3}, & \cos \theta_{y3}, & \cos \theta_{z3} \end{pmatrix}^{-1} \begin{pmatrix} v_{\mathrm{d}1} \\ v_{\mathrm{d}2} \\ v_{\mathrm{d}3} \end{pmatrix}. \tag{43}$$

If we observe more than three directions, then the estimate of $\mathbf{v}$ can be determined in a least-squares manner, with which the residual given by the following is minimized:

$$\varepsilon_v^2 \equiv \sum_{i=1}^{m} (v_x \cos \theta_{xi} + v_y \cos \theta_{yi} + v_z \cos \theta_{zi} - v_{\mathrm{d}i})^2, \tag{44}$$

where $m$ is the number of beam directions. The necessary condition for $\mathbf{v}$ to give the minimum is that partial derivatives of $\varepsilon_v^2$ with respect to all three components of $\mathbf{v}$ are zero:

$$\frac{\partial \varepsilon_v^2}{\partial v_j} = 0 \quad (j = x, y, z). \tag{45}$$

This set of equations can be solved in terms of $\mathbf{v}$ as

$$\mathbf{v} = \begin{pmatrix} \sum \cos^2 \theta_{xi}, & \sum \cos \theta_{xi} \cos \theta_{yi}, & \sum \cos \theta_{xi} \cos \theta_{zi} \\ \sum \cos \theta_{yi} \cos \theta_{xi}, & \sum \cos^2 \theta_{yi}, & \sum \cos \theta_{yi} \cos \theta_{zi} \\ \sum \cos \theta_{zi} \cos \theta_{xi}, & \sum \cos \theta_{zi} \cos \theta_{yi}, & \sum \cos^2 \theta_{zi} \end{pmatrix}^{-1} \begin{pmatrix} \sum v_{\mathrm{d}i} \cos \theta_{xi} \\ \sum v_{\mathrm{d}i} \cos \theta_{yi} \\ \sum v_{\mathrm{d}i} \cos \theta_{zi} \end{pmatrix}, \tag{46}$$

where the summations are taken for $i = 1$ to $m$.

A special case of this type of multi-beam measurements called the *Velocity-Azimuth Display* (VAD) method, which uses beam directions with a fixed zenith angle $\theta$ and uniformly distributed azimuth angles $\phi_i$. The line-of-sight velocity $v_{\mathrm{d}}$ of Eq. 42 is then rewritten as

$$v_{\mathrm{d}i} = v_{\mathrm{h}} \sin \theta \sin(\phi_i + \beta) + v_z \cos \theta, \tag{47}$$

where $v_{\mathrm{h}}$ and $\beta$ are the amplitude and the direction of the horizontal component of $\mathbf{r}$, respectively, and given by

$$v_{\mathrm{h}} = \sqrt{v_x^2 + v_y^2}$$
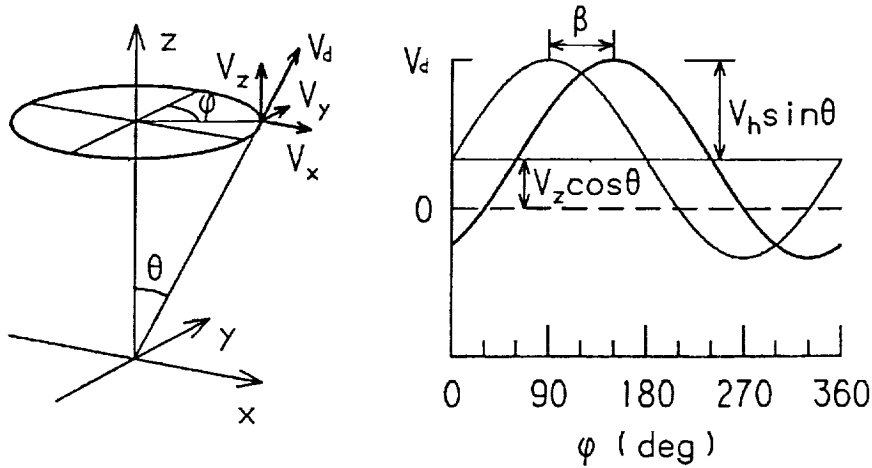$$\beta = \tan^{-1} \left( \frac{v_y}{v_x} \right).$$

**Fig. 9.** Coordinates of the Velocity-Azimuth Display method (left panel), and an expected variation of the line-of-sight velocity $v_d$ as a function of azimuth $\phi$ (right panel).

Figure 9 illustrates coordinates of the VAD method and an expected variation of $v_d$ as a continuous function of azimuth $\phi$. The thin curve on the right panel represents a case where the horizontal component of the velocity is toward the $x$ axis, and the thick line shows a general case.

As understood from this illustration, the vertical component of the velocity is indicated by the DC component, and the horizontal component by the amplitude and the phase of the sinusoid. The fitting procedure given by Eq. 46 thereby reduces to fitting a sinusoid with a DC offset to line-of-sight velocities plotted versus azimuth angle. Any inhomogenuity of the velocity field is indicated by deviations of the curve from a sinusoid.

Although there is nothing superior, in a mathematical sense, of the VAD method compared to other choices of beam directions, there are practical advantages which made the method popular: First, this method is suited for radars with a mechanically steered aperture antenna, of which azimuth and zenith angles are often driven separately. This is the case for most of weather radars, although it is not for phased-array antennas with electrical or electronical steering often used for atmospheric radars.

Secondly, quality of data is readily visualized on a display without numerical computations. Systematic error due to an undesired hard target at some direction, for example, can be picked up easily by human intelligence, but it may require an elaborated software for a computer to find it out.

Thirdly, a systematic error due to specular echoes from the vertical direction can be avoided with the VAD method by choosing the zenith angle $\theta$ properly. The specular echoes from horizontally stratified layers often dominate over isotropic scattering from turbulence (Gage and Green, 1978, Röttger and Liu, 1978), which make the apparent zenith angle of the antenna beam direction smaller than the physical one for beam directions near the vertical direction. This effect is most prominent for lower stratospheric region, where data from beam directions with small zenith angles must be treated with care (Tsuda *et al.*, 1986).

This caution applies, of course, to all DBS observations. On the other hand, use of too large zenith angle makes the assumption of a uniform velocity field unreliable.

The alternate technique of the Spaced-Antenna-Drifts method makes efficient use of this specular echoes in determining horizontal velocities. It was originally developed to study characteristics of irregularities in the lower ionosphere (*e.g.*, Ratcliffe, 1956), and applied to observations of velocities in the middle atmosphere (*e.g.*, Vincent *et al.*, 1977) and lower atmosphere (*e.g.*, Röttger and Vincent, 1978). Its principle is to measure a spatial correlation of received signal patterns from a reflecting layer with spaced antennas on the ground.

For a given angular pattern of the echo power from the reflecting layer, the spatial correlation function on the ground is given by a two-dimensional Fourier transform of the angular pattern as (Ratcliffe, 1956)

$$\rho(x,y) = \int_{-\infty}^{\infty}\int_{-\infty}^{\infty} W(S_1,S_2)\exp\left(2\pi i\frac{S_1 x + S_2 y}{\lambda}\right) dS_1 dS_2, \qquad (48)$$
$$S_1 = \sin\theta_1$$
$$S_2 = \sin\theta_2$$

where $W(S_1,S_2)$ is the power pattern of the echo with respect to the zenith angle $\theta_1$ and $\theta_2$ measured in $x$-$z$ and $y$-$z$ plane, respectively. Note that the integrand takes a real value within a range $(-1,1)$ for $S_1$ and $S_2$. If $W$ is symmetrical with the azimuth angle, which is valid for most of practical cases, Eq. 48 can be rewritten in a polar coordinates $(\theta,\phi)$ as

$$\rho(\alpha) = \int_0^\infty \int_{-\pi}^\pi W(S)\exp(2\pi i\alpha S\cos\phi)Sd\phi dS, \qquad (49)$$

where $S = \sin\theta$, and $\alpha = \sqrt{(x^2 + y^2)}/\lambda$ is a distance measured in units of the wavelength. The integral with respect to $\phi$ is the Bessel function of zero order $J_0(2\pi\alpha S)$ so that

$$\rho(\alpha) = 2\pi \int_0^\infty W(S)J_0(2\pi\alpha S)SdS. \qquad (50)$$

For randomly distributed irregularities in a thin horizontal layer at a height $z = h$, the power flux in the angular range $\theta$ to $\theta + d\theta$ depends only on the antenna pattern of
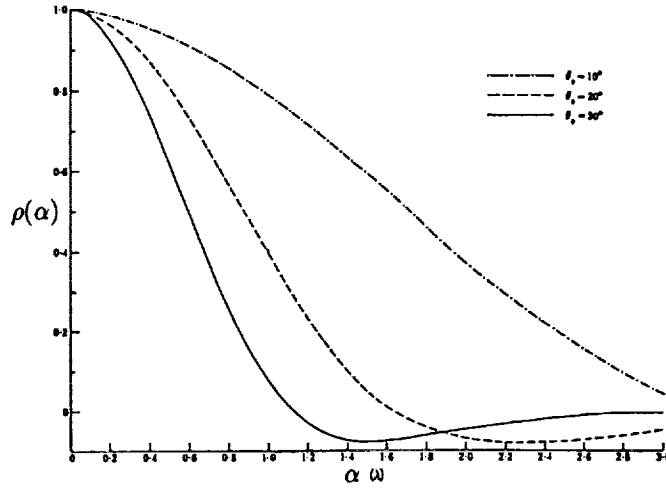
48



**Fig. 10.** normalized correlation function $\rho(\alpha)$ between fluctuations recorded by two receivers separated by a distance $\alpha$. It is assumed that the irregularities are isotropic and randomly distributed, and that both the transmitting and receiving antennas have a pattern of $\exp(-\sin^2\theta/\sin^2\theta_o)$ (after Briggs and Vincent, 1973).

the transmitting and receiving antennas, and given by (Briggs and Vincent, 1973)

$$W(\theta)d\theta \propto h^{-2}T(\theta)R(\theta)\sin\theta\cos\theta d\theta, \tag{51}$$

where $T(\theta)$ and $R(\theta)$ are the transmitting and receiving antenna patterns, respectively. Figure 10 draws examples of the correlation function for Gaussian antenna patterns with different width, but assuming the same pattern both for transmission and reception (after Briggs and Vincent, 1973).

We have so far considered the spatial correlation only. As implied by Eq. 41, the received signal is also characterized by its temporal correlation function, which is a Fourier transform of the frequency power spectrum. The spatial and temporal correlations can be treated separately for the case of a stationary pattern, while they are mutually related when the layer, and hence the pattern, has a mean motion. A generalized method called the *full-correlation analysis* was developed by Briggs (1984) in order to retrieve the velocity and other information from such correlation functions. We now introduce the space-time correlation function of the received signal pattern $f(x,y,t)$ on the ground plane:

$$\rho(\xi,\eta,\tau) = \frac{\langle f(x,y,t)f(x+\xi,y+\eta,t+\tau)\rangle}{|f(x,y,t)|^2}, \tag{52}$$

where $()$ means to take an ensemble average, which is often replaced by a temporal average in practical applications. This correlation function represents the statistical relations of the signal pattern at two points with a separation $(\xi, \eta)$ on the ground and with a time difference of $\tau$. We assume that for a stationary pattern, the correlation function has a form

$$\rho(\xi, \eta, \tau) = \rho(A\xi^2 + B\eta^2 + K\tau^2 + 2H\xi\eta). \tag{53}$$

This assumption implies that the spatial and temporal correlations have the same functional shape, but the shape is arbitrary. Although this is not real in a rigorous sense, it is an acceptable approximation for most of correlation functions at least around their origin.

We next suppose that the pattern is moving at a velocity $\mathbf{V} = (V_x, V_y)$. If we move the coordinates also at this velocity, then Eq. 53 remain unchanged for the moving coordinates. the expression for the stationary coordinates is therefore obtained after a linear transform of coordinates that

$$\rho(\xi, \eta, \tau) = \rho\{A(\xi - V_x\tau)^2 + B(\eta - V_y\tau)^2 + K\tau^2 + 2H(\xi - V_x\tau)(\eta - V_y\tau)\}, \tag{54}$$

which is rewritten as

$$\rho(\xi, \eta, \tau) = \rho(A\xi^2 + B\eta^2 + K\tau^2 + 2F\xi\tau + 2G\eta\tau + 2H\xi\eta). \tag{55}$$

If we have two spaced receivers, we can determine the shape of the cross-correlation as a function of $\tau$ for a given set of $(\xi, \eta)$. Since Eq. 55 is a function of a second-order polynomial of $\tau$, it is possible to determine three unknowns by fitting it to the measured cross-correlation function. It is thus clear that three spaced receivers, which provides us two sets of independent cross-correlation functions, is sufficient to determine all coefficients in Eq. 55. If we have more than three receivers, we can determine the coefficients in a least-squares manner as is the case of the DBS method.

Once the coefficients are determined, we can retrieve the velocity vector $\mathbf{V}$ from these coefficients. By comparing Eqs. 54 and 55, we obtain

$$\begin{aligned} AV_x + HV_y &= -F \\ BV_y + HV_x &= -G \end{aligned} \tag{56}$$

These equation can be readily solved to give $(V_x, V_y)$. The vertical component of the velocity vector needs to be determined separately from the Doppler shift of the echo.

An important point which needs to be mentioned is that an apparent velocity $V'$ calculated from the distance between the receivers and the time delay which gives the maximum value of the cross-correlation function does not agree with the true velocity
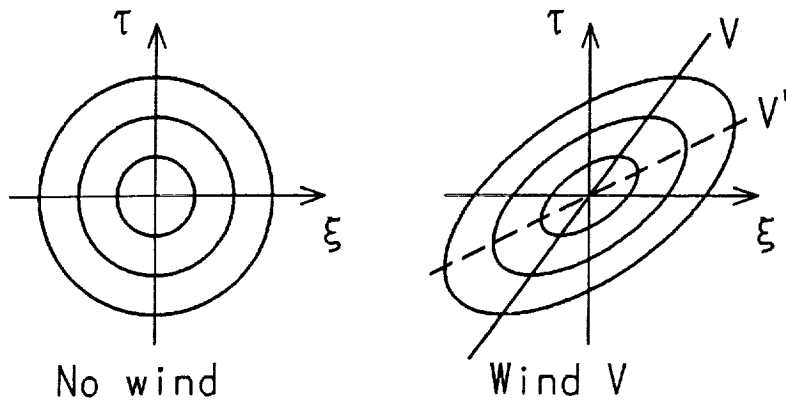
**Fig. 11.** Contours of equal correlation versus distance $\xi$ and time delay $\tau$. The left panel shows a case with no mean wind, and the right panel is with a uniform wind. The true velocity $V$ estimated with the full-correlation analysis is denoted by the solid line. The dashed line indicates the apparent velocity $V'$ determined from the time delay of maximum correlation.

$V$ of the pattern, which is correctly estimated with the full-correlation analysis. These two time delays coincide when the temporal correlation of the pattern is perfect, which means that the pattern is drifting without evolving with time, while a finite correlation time significantly affects the shape of the cross-correlation function.

Figure 11 illustrates this difference schematically. The left panel shows concentric circles which represent contour lines of equal correlation versus distance $\xi$ along the baseline and the time delay $\tau$ for a case of no mean motion. The abscissa and the ordinate are normalized by the correlation distance and the correlation time of the pattern, so that the contours become circles instead of ellipses. If a mean motion of $V$ is added, the contours deform into ellipses as shown in the right panel. Note that the solid line which indicates the true velocity $V$ is drawn by connecting tangential points of the ellipses with horizontal lines as implied by Eq. 54.

Since the cross-correlation function with respect to $\tau$ at a distance $\xi$ is given by the values of contours along a line of constant $\xi$ (*i.e.*, a vertical line), $V'$ obtained from its maximum has a slope indicated by the dashed line in the figure, which is drawn by connecting tangential points of ellipses with vertical lines. The difference between the true velocity $V$ and the apparent velocity $V'$ therefore becomes larger as $V$ becomes smaller. One of reasons that the full-correlation analysis is widely used is that it is free from this
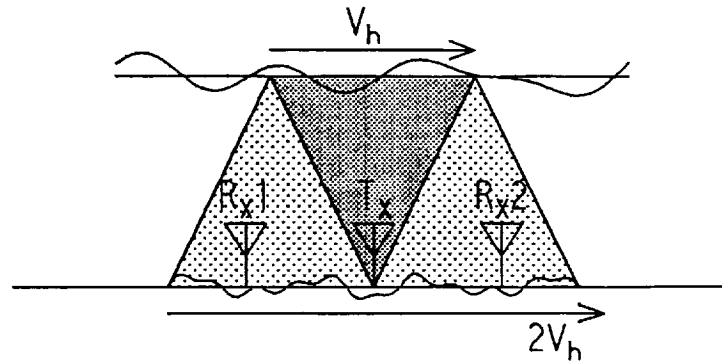
**Fig. 12.** Motion of a reflecting layer and its echo pattern on the ground.

:ind of error.

We should also note that the velocity **V** we have discussed is the velocity of the pattern ɔn the ground, which is exactly *twice* that of the layer as schematically shown in Figure 12. This is intuitively understood by considering the motion of a shadow of a screen projected on a wall where the light source, the screen and the wall are arranged with equal intervals. It is, of course, possible to derive this relation mathematically by examining the motion of an interference pattern on the ground due to echoes from two or more targets moving horizontally at the same velocity.

From a practical point of view, the DBS and SAD methods have their own advantages and disadvantages which are difficult to compare on the same ground. The advantages of the SAD method are that the complete velocity vector can be determined from a single volume of the target, and that the enhanced specular echoes from the vertical direction can be used efficiently. However, it requires at least three sets of receiving antennas and receivers with equal capability. The DBS method requires, on the other hand, a steerable antenna, which is not necessary with the SAD method. The accuracy of the velocity estimates is known fairly well for the DBS method, while it has not yet been studied in details for the SAD method, which is anticipated to have a variable accuracy depending on the velocity itself.

# References

Balsley, B. B., and K. S. Gage, The MST radar technique: Potential for middle atmospheric studies, *Pure Appl. Geophys.*, **118**, 452-493, 1980.

Battan, L. J., *Radar Observation of the Atmosphere*, The University of Chicago Press, Chicago, 1973.

Briggs, B. H., The analysis of spaced sensor records by correlation technique, *Handbook for MAP*, **13**, 166-186, 1984.

Briggs, B. H., and R. A. Vincent, Some theoretical considerations on remote probing of weakly scattering irregularities, *Aust. J. Phys.*, **26**, 805-814, 1973.

Dicke, R. H., R. Beringer, R. L. Kyhl, and A. B. Vane, Atmospheric absorption measurements with a microwave radiometer, *Phys. Rev.*, **70**, 340-348, 1946.

Doviak, R. J., and D. S. Zrnić, *Doppler Radar and Weather Observations*, Academic Press, London, 1984.

Farley, D. T., Multi-pulse incoherent-scatter correlation function measurements, *Radio Sci.*, **4**, 935-953, 1969.

Fejer, J. A., Scattering of radio waves by an ionized gas in thermal equilibrium in the presence of a uniform magnetic field, *Can. J. Phys.*, **39**, 716-740, 1961.

Friend, A. W., Theory and practice of tropospheric sounding by radar, *Proc. Inst. Radio Eng.*, **37**, 116-138, 1949.

Gage, K. S., and J. L. Green, Evidence for specular reflection from monostatic VHF radar observations of the stratosphere, *Radio Sci.*, **13**, 991-1001, 1978.

McKinley, D. W. R., *Meteor Science and Engineering*, McGraw-Hill, New York, 1961.

Mechtly, E. A., S. A. Bowhill, K. P. Gibbs, and L. G. Smith, Changes of lower ionosphere electron concentrations with solar activity, *J. Atmos. Terr. Phys.*, **34**, 1899-1907, 1972.

Nathanson, F. E., *Radar Design Principles*, McGraw-Hill, New York, 1969.

Ratcliffe, J. A., Some aspects of diffraction theory and their application to the ionosphere, *Rep. Progr. Phys.*, **19**, 188-267, 1956.

Röttger, J., and C. H. Liu, Partial reflection and scattering of VHF radar signals from the clear atmosphere, *Geophys. Res. Lett.*, **5**, 357-360, 1978.

Röttger, J., and R. A. Vincent, VHF radar studies of tropospheric velocities and irregularities using spaced antenna techniques, *Geophys. Res. Lett.*, **5**, 917-920, 1978.

Silver, S., *Microwave Antenna Theory and Design*, McGraw-Hill, New York, 1951.

Skolnik, M. L. (editor), *Radar Handbook*, McGraw-Hill, New York, 1970.

Skolnik, M. L., *Introduction to Radar Systems*, McGraw-Hill, New York, 1980.

Stix, T. H., *The Theory of Plasma Waves*, McGraw-Hill, New York, 1962.

Tsuda, T., T. Sato, K. Hirose, S. Fukao, and S. Kato, MU radar observations of the aspect sensitivity of backscattered VHF echo power in the troposphere and lower stratosphere, *Radio Sci.*, **21**, 971-980, 1986.

Vincent, R. A., T. J. Stubbs, R. H. O. Pearson, K. H. Lloyd, and C. H. Low, A comparison of partial reflection drifts with winds determined by rocket techniques – I, *J. Atmos. Terr. Phys.*, **39**, 813-821, 1977.